The International Journal of Advanced Manufacturing Technology (2019) 102:55–65
https://doi.org/10.1007/s00170-018-3167-3

ORIGINAL ARTICLE

Investigating the effects of external magnetic field on machining characteristics of electrical discharge machining process, numerically and experimentally

Mohammad Reza Shabgard[1] · Ahad Gholipoor[1] · Mousa Mohammadpourfard[2]

Received: 6 July 2018 / Accepted: 7 December 2018 / Published online: 19 December 2018

Abstract
Application of external magnetic field in electrical discharge machining is one of the methods to increase this process capability and decrease its limitations. In the present study, a single discharge in magnetic field-assisted electrical discharge machining has simulated using finite element method in order to obtain the temperature distribution and generated crater dimensions on the workpiece surface. A new mathematical model for plasma channel radius was also developed and used at simulation stage. Regarding good agreement between recast layer thickness obtained by numerical and experimental methods with maximum error of 8.8%, the effects of applying external magnetic fields on plasma flushing efficiency and recast layer thickness were found numerically and experimentally. Also the influences of pulse current and pulse on-time on dimensions of generated craters at magnetic field-assisted EDM were studied numerically. The results showed the positive effects of application of external magnetic field in EDM process on increasing plasma flushing efficiency and decreasing recast layer thickness.

Keywords Electrical discharge machining · External magnetic field · Numerical analysis · Mathematical modeling
Plasma flushing efficiency · Recast layer thickness

1 Introduction

Several investigators studied application of magnetic field in finishing process in order to decrease surface roughness (SR) in recent decade [1–3]. Also some investigators applied magnetic field around gap distances at electrical discharge machining (EDM) for solving the EDM restrictions [4].

Bruijn et al. [5] studied magnetic field-assisted EDM (MEDM) process in 1978, firstly. Application of magnetic field in EDM process causes better debris flushing from gap distance, reduction of gap pollution, decreasing the number of abnormal pulses, and increasing the machining performance [6, 7]. Lin et al. [8] compared discharge waves, material removal rate (MRR), tool wear rate (TWR), surface roughness, and surface integrity obtained by EDM and magnetic field-assisted EDM processes and resulted that due to improving debris removal from machining gap and reducing gap pollution by applying magnetic field, the MEDM process leads to lower abnormal pulses like arc, more MRR, and lower surface roughness but a little more TWR. Lin et al. [9] compared EDM and MEDM processes. According their results, the MEDM process leads to better machining stability. They found that lower micro-cracks with thinner recast layer are created at workpiece surface in the case of MEDM process. Govindan et al. [10] studied the material removal at single discharge of dry EDM process along with magnetic field, numerically and experimentally. They investigated the influences of process inputs containing pulse current, voltage, magnetic field intensity, and pulse on-time on crater dimensions generated on workpiece surface experimentally. According to their results, application of magnetic field in dry EDM decreases generated crater diameter and increases crater depth on workpiece surface. Joshi et al. [11] applied an external magnetic field around gap distance at dry EDM and resulted that due to increasing the plasma density in this hybrid method, the MRR increases up to 130%. They found that applying magnetic field decreases the overcut at dry EDM

✉ Mohammad Reza Shabgard
mrshabgard@tabrizu.ac.ir

[1] Mechanical Engineering Department, University of Tabriz, Tabriz, Iran

[2] Faculty of Chemical and Petroleum Engineering, University of Tabriz, Tabriz, Iran

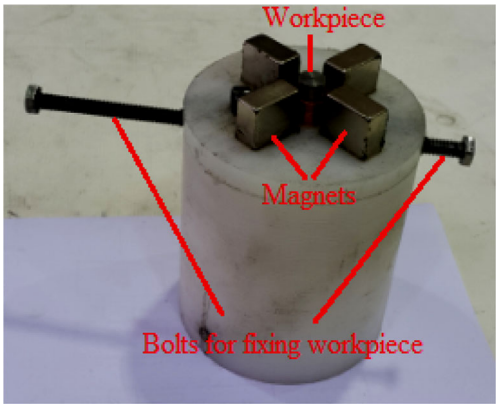

Fig. 1 The fixture used for applying magnetic field

process. Kao et al. [12] applied external magnetic field around gap distance of EDM process in machining of small holes and resulted that with this approach, MRR is increased and TWR is decreased. Heinz et al. [13] applied an external magnetic field around gap distance of EDM process in machining of non-magnetic materials.

In this investigation, a finite element model (FEM) was developed for a single discharge of MEDM process to investigate the effects of applying magnetic field around gap distance on plasma flushing efficiency (PFE) and recast layer thickness (RLT), experimentally and numerically.

2 Experiments

2.1 Experimental setup

The fixture which was shown at Fig. 1 was designed for workpiece to apply magnetic field around gap distance of EDM process. Also Fig. 2 shows the spark machine (CHARMILLES ROBOFORM 200) with fixture for applying magnetic field which was used in this investigation.

The fixture material was plastic while four neodymium permanent magnets with intensity of 1.3 T and dimensions of 25 × 20 × 10 mm were located at their positions at fixture according to Fig. 1 (the distance between the edge of magnets with workpiece was considered 2 mm, while magnetic field intensity at the edge of workpiece was 0.3 T). Also, magnetic field lines caused by this kind of alignment of magnets around the gap distance are similar to Fig. 3. Neodymium permanent magnets have higher magnetic strength with small sizes which makes the usage of these kinds of magnets expands rapidly.

It is necessary to mention that the shape, dimensions, magnetic field intensity, and the number and position of magnets at MEDM process were determined by performing exploratory tests regarding the obtaining of the maximum MRR as output parameter.

2.2 Experimental procedure

In this study, the influence of application of magnetic field in EDM process on PFE and generated RLT on machined surface was investigated by selecting pulse current and pulse on-time as input parameters of EDM and MEDM processes because of their importance [14], (each one in four levels) and performing 16 experiments for each process (according to full factorial method) and comparing the results of MEDM with EDM process.

Regarding some exploratory experiments which were performed and reviewing other studies [15], the variables and fixed input parameter levels were determined according to Table 1. The time of each experiment was considered 10 min and a new tool electrode was used for each experiment.

Recording different types of MEDM process pulses was done by employing a Hitachi VC-6524 oscilloscope. Counting the number of normal pulses was done by using the written MATLAB code.

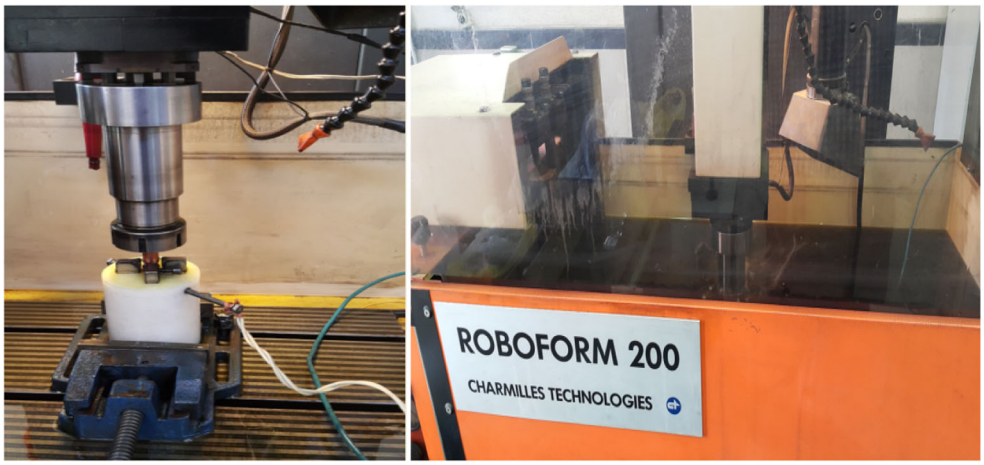

Fig. 2 Spark machine with special fixture for applying magnetic field around gap distance which was used at MEDM process

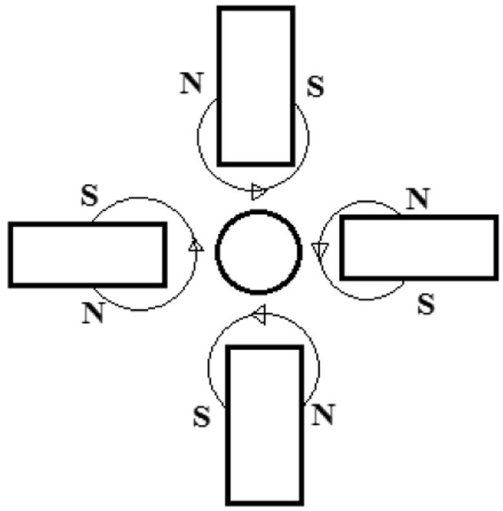

Fig. 3 Magnetic field lines induced by the alignment of magnets around the gap distance

A CP2245-Sartorius digital balance with 0.1-mg resolution was used to measure the workpiece weight before and after machining process.

The machined surface by MEDM process was cut transversely; then, the metallographic and etching operations were done, in order to measure the created RLT on machined surface by using a VEGA\\TESCAN scanning electron microscopy. The RLT was measured in 20 different points and their average considered as the RLT.

2.3 Experimental materials

AISI H13 tool steel has high tension strength (1400–1750 N/mm^2) which leads to high malleability of this steel. High toughness and resistance against wear, thermal cracking, fatigue, and corrosion are other key properties of H13 tool steel. This steel keeps its hardness up to 425 °C and the tools manufactured from this steels can work up to 540 °C [16]. Cylindrical H13 hot work tool steel, 10 mm in diameter and 20 mm in height, with grinded and polished surfaces was selected as workpiece materials.

Table 1 The input parameters of this study and their levels

Parameter	Level
Peak current (A)	4, 8, 16, 32
Pulse on-time (μs)	6.4, 12.8, 50, 100
Pulse interval (μs)	6.4
Open-circuit voltage (V)	200
Gap distance (μm)	50
Polarity	Positive
Flushing type	Normal submerged on Oil Flux ELF as dielectric

The tool material in this study was copper with 99% purity. In this process, the tool was cylinder with 14 mm in diameter and 40 mm in height which was manufactured by turning operation.

3 Finite element simulation

3.1 Mathematical principles

The differential equation for heat transfer during each discharge of MEDM process without term of internal heat generation is according to Eq. 1 [17]:

$$\rho c_P \frac{\partial T}{\partial t} = k\left[\frac{1}{r}\frac{\partial}{\partial r}\left(r\frac{\partial T}{\partial r}\right) + \frac{\partial}{\partial z}\left(\frac{\partial T}{\partial z}\right)\right] \tag{1}$$

where ρ is workpiece density, k is thermal conductivity coefficient of the workpiece, C_p is specific heat capacity, t is time, T is temperature, and r and z are coordinate axis as shown in Fig. 4. Equation 1 is the base of thermal modeling to achieve the heat distribution during each discharge of MEDM process.

The considered domain for applying boundary conditions of workpiece during pulse on-time of MEDM process is showed in Fig. 4. These boundary conditions are according to Eqs. 2 and 3.

The boundary conditions of boundaries 3 and 4:

$$k\frac{\partial T}{\partial z} = \begin{cases} h_f(T-T_0) & \text{for} \quad r > R \\ q(r) & \text{for} \quad r < R \end{cases} \tag{2}$$

The boundary conditions of boundaries 1, 2, and 5:

$$k\frac{\partial T}{\partial z} = 0 \tag{3}$$

where $q(r)$ is the quantity of heat flux entering to the workpiece and tool and R is the plasma channel radius.

The initial temperature of electrodes can be taken as equal as the temperature T_0 which is environment temperature.

The following assumptions also have been considered:

- Only one spark occurs for one discharge.
- The workpiece electrode is considered as a semi-infinite body.
- The thermo-physical properties of workpiece are considered as independent of temperature.
- The workpiece material is homogenous and isotropic.
- Heat incident on the workpiece is dissipated by conduction into the workpiece while heat transfer is by convection at workpiece-dielectric liquid interface.
- The generated recast layer is considered to be uniform.
- A part of total discharge energy is transferred to workpiece.

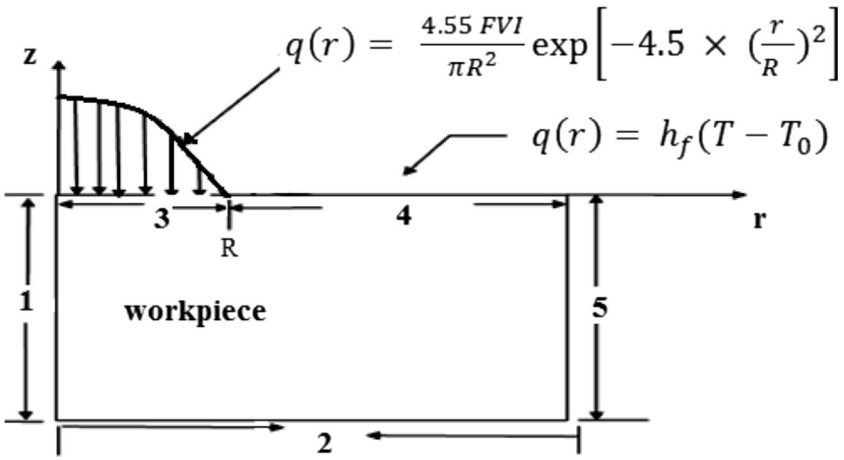

Fig. 4 Schematic of thermal model of MEDM

Because of more precise results obtained by Gaussian heat distribution in compared with other heat sources [18, 19], it was applied for heat transfer analysis. Equation 4 demonstrates the heat flux $q(r)$ at radius r [20].

$$q(r) = \frac{4.55\ F_c VI}{\pi R_p^2} \exp\left[-4.5\ \left(\frac{r}{R}\right)^2\right] \tag{4}$$

where V is the discharge voltage, I is the pulse current, F_c is the part of the total energy transferred to the workpiece, and R is the plasma channel radius.

The fraction of total energy transferred to the workpiece was considered 34% [21], 18% [22], 14% [23], and 50% [17, 24, 25] in different studies about EDM process. In this investigation, the relation which was developed by Shabgard et al. for this purpose [26], (Eq. 5) was used to determine F_c.

$$F_c = 5.5998 \times I^{-0.3401} \times \mathrm{Ton}^{0.2989} \tag{5}$$

In this study, mathematical modeling was used to define the radius of plasma channel. So regarding Fig. 5 which shows the schematic of acting forces on plasma channel, a differential equation was developed for this purpose (Eq. 6).

$$\frac{\mathrm{d}^2 \mathrm{r}}{dt^2} = \frac{\mathrm{eq}}{2\pi \mathrm{r} \mathrm{d} \varepsilon_0 \mathrm{m}} - \frac{e\vartheta B_s}{m} - \frac{e\vartheta B_E}{m} + \frac{P_{in}(2rd)}{m} - \frac{P_{\mathrm{out}}(2rd)}{m} - \frac{\gamma(2r+2d)}{m} \tag{6}$$

In Eq. 6 which was obtained by balancing of the forces affecting the plasma channel, $\frac{d^2r}{dt^2}$ is plasma channel radial expanding acceleration. All of the terms in the right side of equations are the plasma channel radial acceleration, where the phrase of $\frac{\mathrm{eq}}{2\pi r d \varepsilon_0 \mathrm{m}}$ is because of electric field caused by the presence of charged particles within plasma channel. The

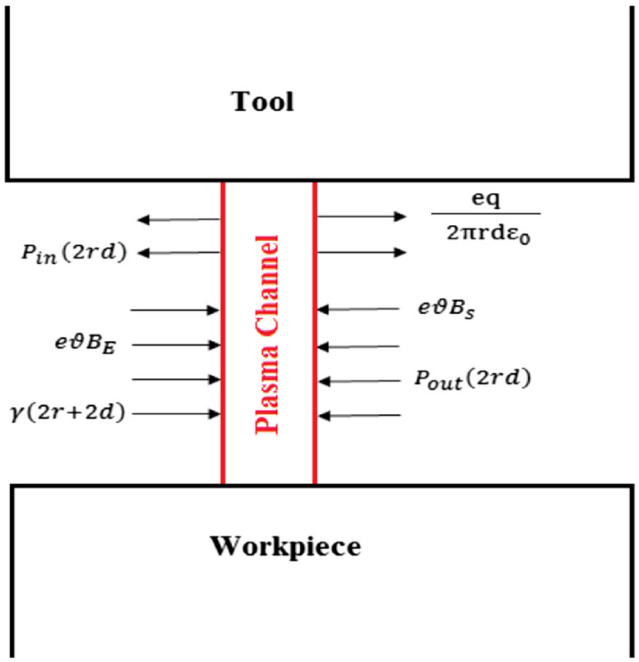

Fig. 5 The schematic of acting forces on plasma channel

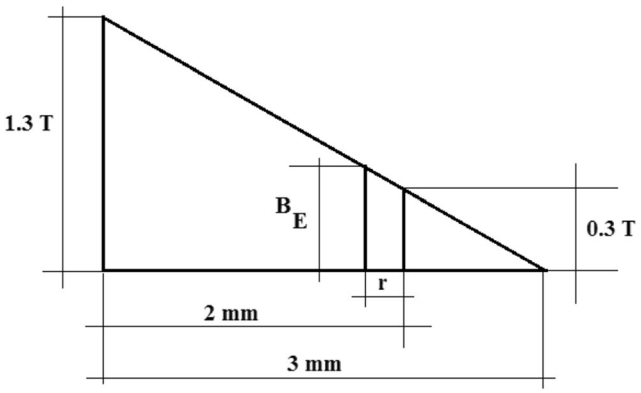

Fig. 6 The method of finding the magnetic field intensity at the between plasma channel and dielectric interface with distance of "r" from the edge of the workpiece

$\frac{e\vartheta B_s}{m}$ phrase is because of created magnetic field around plasma channel caused by charged particles movement within plasma channel. The phrase of $\frac{e\vartheta B_E}{m}$ is because of applying external magnetic field around gap distance. The phrase of $\frac{P_{in}(2\mathrm{rd})}{m}$ is because of the force induced by internal pressure of plasma channel. The $\frac{P_{\mathrm{out}}(2\mathrm{rd})}{m}$ phrase is because of the force induced by external pressure of dielectric on plasma channel. The phrase of $\frac{\gamma(2r+2d)}{m}$ is because of the surface tension at plasma channel and dielectric interface.

In Eq. 6, r is plasma channel radius, t is pulse on-time, e is the electrical charge of the electron, q is the charged particles within plasma channel and is determined by Eq. 7 [27], d is gap distance, ε_0 is vacuum permittivity, m is plasma channel mass ($m = 2 \times 10^{-12}$ kg) [28], ϑ is drift velocity of charged particles within plasma channel and is determined with Eq. 8 [29], B_s is the generated magnetic field around plasma channel because of movement of charged particles within plasma channel and is determined by Eq. 9 [27], B_E is the applied external magnetic field around plasma channel and is determined with Eq. 10 at plasma channel and dielectric interface with distance of "r as plasma channel radius" from the edge of the workpiece (as shown in Fig. 6, and regarding to Thales's theorem and considering that the magnetic field intensity at the edge of the magnets is 1.3 T, at the edge of the workpiece (located in 2 mm from the edge of the magnets) is 0.3 T and in the distance of 3 mm from the edge of the magnets is approximately zero). P_{in} is internal pressure of plasma channel and is determined with Eq. 11 [30]. P_{out} is external pressure of dielectric influenced on plasma channel and is determined with Eq. 12. γ is generated surface tension at plasma channel and dielectric interface ($\gamma = 32 \times 10^{-3}$ N/m) [31, 32].

$$q = ne \tag{7}$$

In Eq. 7, n is the number of charged particles within plasma channel and is defined with Eq. 13 [33].

$$\vartheta = \frac{V}{V_m} \times 10^4 \tag{8}$$

In Eq. 8, V_{m} is mean discharge voltage at EDM process.

$$B_s = \frac{\mu_0 i}{2\pi r} \tag{9}$$

In Eq. 9, μ_0 is vacuum magnetic permeability.

$$B_E = 0.3 + 0.43r \tag{10}$$

$$P_{\mathrm{in}} = (n_e + n_i)k_B T - \Delta P \tag{11}$$

In Eq. 11, n_e and n_i is the number of electrons and ions in plasma channel, k_B is the Boltzmann's constant, T is the temperature of plasma channel temperature ($T = 10{,}000$ °C) [34], and ΔP is an index to show non-ideality of plasma channel and is defined with Eq. 14 [35].

$$P_{\mathrm{out}} = P_0 + \rho g h \tag{12}$$

In Eq. 12, P_0 is air pressure, ρ is dielectric density, g is earth gravity, and h is dielectric height from sparking point up to dielectric surface.

$$n_e = \frac{j}{e\left(\frac{k_B T_e}{m_e}\right)^{0.5}} \tag{13}$$

In Eq. 13, j is current density, T_e is the electron temperature, and m_e is the electron mass.

$$\Delta P = \frac{e^2}{24\pi\varepsilon_0 \lambda_D}(n_e + n_i) \tag{14}$$

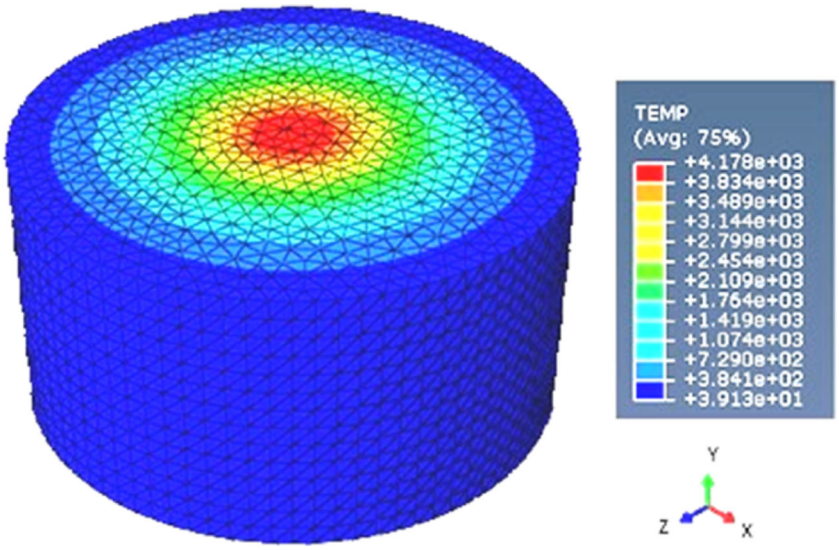

Fig. 7 Application of FEM at modeling of a single discharge of MEDM process

In Eq. 14, λ_D is the Debye length and is determined by Eq. 15 [36].

$$\lambda_D = \left(\frac{\varepsilon_0 k_B T}{n_e e^2}\right)^{\frac{1}{2}} \tag{15}$$

The ABAQUS/CAE which is standard finite element software was applied to simulate the MEDM process and implement a thermal analysis to find the temperature distribution on machined surface. This software is able to consider the temperature dependent properties of material which increases the accuracy of finite element model. So the time-dependent properties of material (conductivity, density, elastic, specific heat, and latent heat) are used at finite element simulation of EDM process.

The element type in the finite element analyses was 10 node tetrahedron meshes with the size of 10 mm, approximately. Also a "dflux" subroutine was written in FORTRAN compiler to apply the heat flux developing with time during pulse on-time. The temperature profiles obtained by FEM analysis was used to calculate the crater dimensions on machined surface [37]. Also the melting latent heat of workpiece which has the significant effect on the simulation results was considered at finite element simulation. Figure 7 shows the application of FEM at modeling of a single discharge of MEDM process.

3.2 Model validation

Comparing experimental recast layer thickness (RLT_{EXP}) and the numerical recast layer thickness (RLT_{Num}) at various settings was the methodology of validation of numerical analysis, in this investigation. This comparison was shown at Table 2 and demonstrates good agreement between numerical and experimental results, with maximum error of 8.8%. RLT_{EXP} was obtained as mentioned before and RLT_{Num} were obtained as below.

The efficiency of material removal from workpiece surface is defined with PFE. PFE is described by Eq. 16 [38].

$$\%\mathrm{PFE} = 100 \times \frac{V_C(\mathrm{EXP})}{V_C(\mathrm{FEM})} \tag{16}$$

where PFE is the plasma flushing efficiency, V_C(FEM) is the theoretical melted material volume per pulse, and V_C(EXP) is the experimental removed material volume per pulse.

Equation 17 defines the theoretical volume of crater obtained by finite element analysis.

$$Vc(\mathrm{FEM}) = \frac{1}{2}\,\pi \mathrm{D_C R_C^2} \tag{17}$$

where D_C and R_C are the depth and radius of the generated craters on workpiece surface.

Figure 8 is a sample of temperature distribution profiles obtained by FEM in line with depth and radius of workpiece during single discharge of MEDM process and demonstrate the temperature of different points of workpiece. The isothermal points with melting point of workpiece were considered as boundary of generated craters in line with depth and radius (depth and radius of craters).

The experimental removed material volume per pulse is obtained by Eq. 18.

$$Vc(\mathrm{EXP}) = \frac{(M_1 - M_2)}{(\mathrm{NN} \times \rho)} \tag{18}$$

where M_1 and M_2 are the workpiece weight before and after machining, NN is the number of normal pulses during a machining period, and ρ is the density of workpiece.

The numerical value of recast layer thickness (RLT_{Num}) has been calculated through Eq. 19:

$$\mathrm{RLT_{Num}} = D_C - \%\mathrm{PFE} \times D_C \tag{19}$$

4 Results and discussion

4.1 Influences of applying magnetic field on PFE

Figure 9a–d shows the influences of applying external magnetic field around gap distance of EDM on plasma channel efficiency in various pulse current and pulse on-times. According to Fig. 9 which compared the PFE of EDM and MEDM processes, it is clear that the PFE of MEDM process is more than EDM in all pulse currents and on-times.

Table 2 Experimental and numerical RLT at MEDM process

I (A)	T_{on} (μs)	$V_{c\ EXP}$ (μm^3)	$V_{c\ FEM}$ (μm^3)	PFE%	RLT_{EXP} (μm)	RLT_{NUM} (μm)	Error%
8	12.8	2689.2455	7484.68	35.93	6.76	7.19	5.9
16	12.8	6871.81	13,164.4	52.2	7.2	6.86	4.9
32	12.8	12,219.44	23,912.8	51.1	8.27	7.56	8.5
8	50	15,740.78	42,144	37.35	11.94	12.27	2.6
16	50	38,419.68	74,226.6	51.76	12.5	12.2	2.4
32	50	79,616.52	141,089	56.43	13.4	12.21	8.8

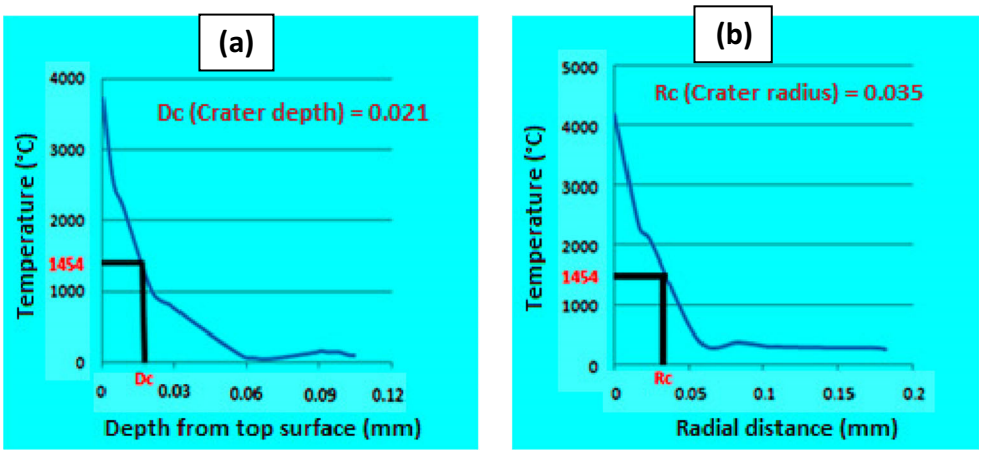

Fig. 8 Temperature distribution in **a** depth and **b** radial direction of workpiece at single discharge of MEDM ($I = 8$ A, $T_{on} = 50$ μs)

Application of magnetic field in EDM has direct impact on the amount of repulsed molten materials from molten puddle and PFE.

Application of magnetic field leads to better debris removal from gap distance which leads to decrease in gap pollution. Fewer number of occurred arc pulses in the case of MEDM process in comparison with EDM, according to Fig. 10, indicates this issue. Lower gap pollution leads to lower plasma channel radius and area, which increases the density of discharged energy. Also application of magnetic field in EDM process confines the plasma channel development due to creation of Lorentz force which is acted on plasma channel according to Eq. 6.

Considering these issues, the plasma channel temperature and so the pressure and its gradient is increased and considering bulk boiling mechanism of MRR, the PFE is increased by application of magnetic field in EDM process.

4.2 Influences of applying magnetic field on the RLT

According to Fig. 11a–d, which compares the amount of generated RLT on machined surface in different pulse currents and pulse on-times in MEDM and EDM processes, the amount of generated RLT is lower in the case of MEDM

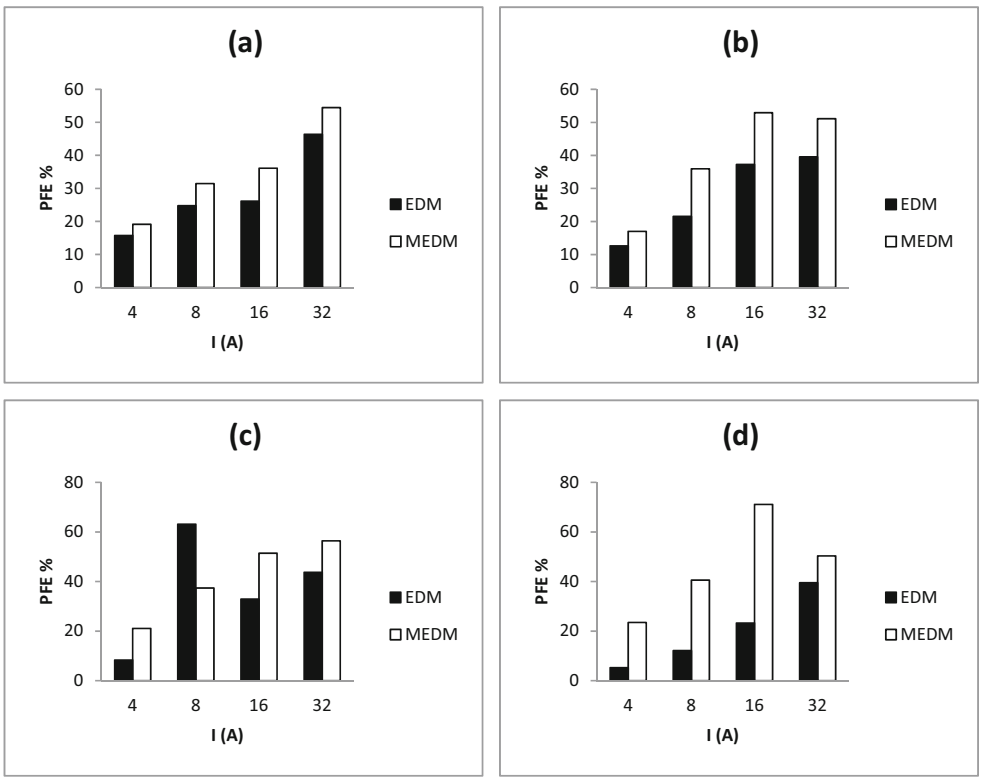

Fig. 9 The influences of application of external magnetic field in EDM process on the PFE in different pulse current in **a** $T_{on} = 6.4$ μs, **b** $T_{on} = 12.8$ μs, **c** $T_{on} = 50$ μs, and **d** $T_{on} = 100$ μs

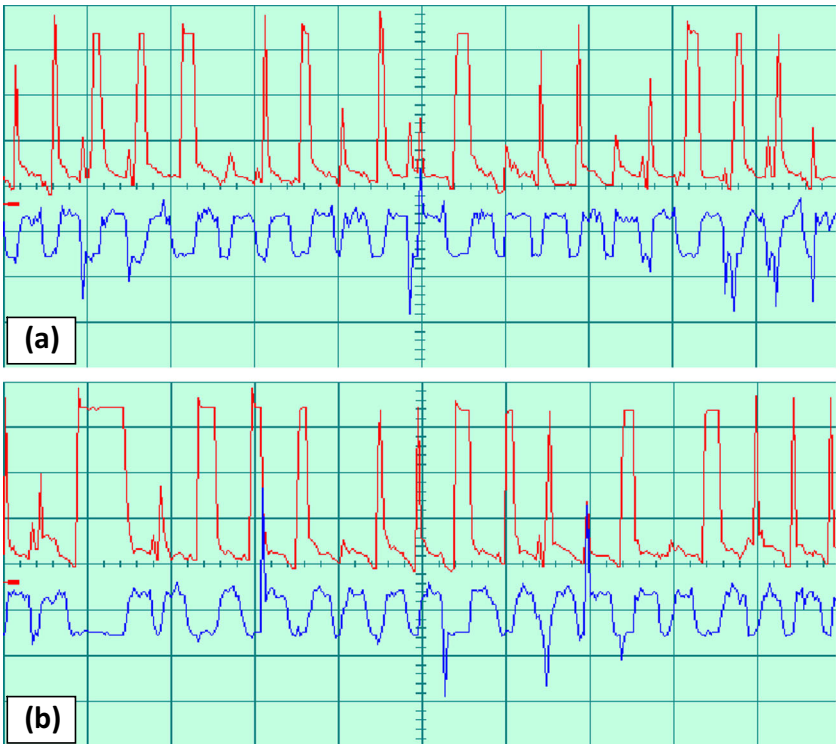

Fig. 10 Voltage and current pulses at $I = 16$ A and $T_{on} = 50$ μs. **a** EDM process and **b** MEDM process

process as compared with EDM process in all pulse currents and pulse on-times.

The PFE is increased by application of magnetic fields in EDM process, and so the amount of molten materials flushed away from molten puddle is increased and the amount of molten material which is re-solidified and attached to machined workpiece and generated recast layer, is decreased.

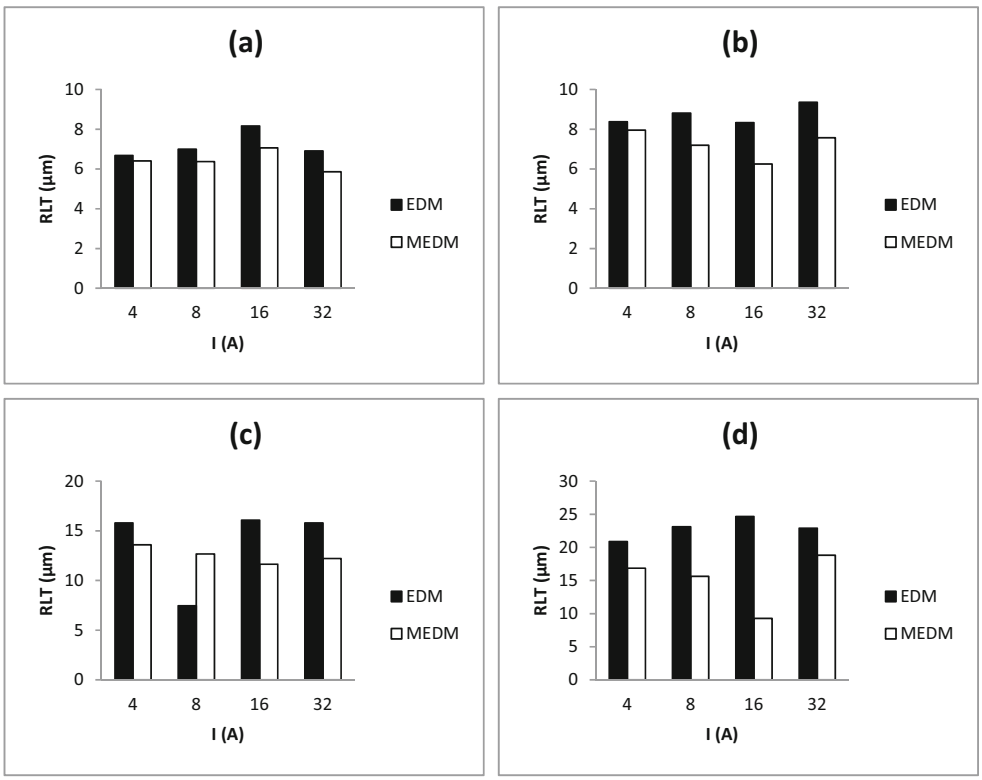

Fig. 11 The effects of application of external magnetic fields in EDM process on the RLT in different pulse current in **a** $T_{on} = 6.4$ μs, **b** $T_{on} = 12.8$ μs, **c** $T_{on} = 50$ μs, and **d** $T_{on} = 100$ μs

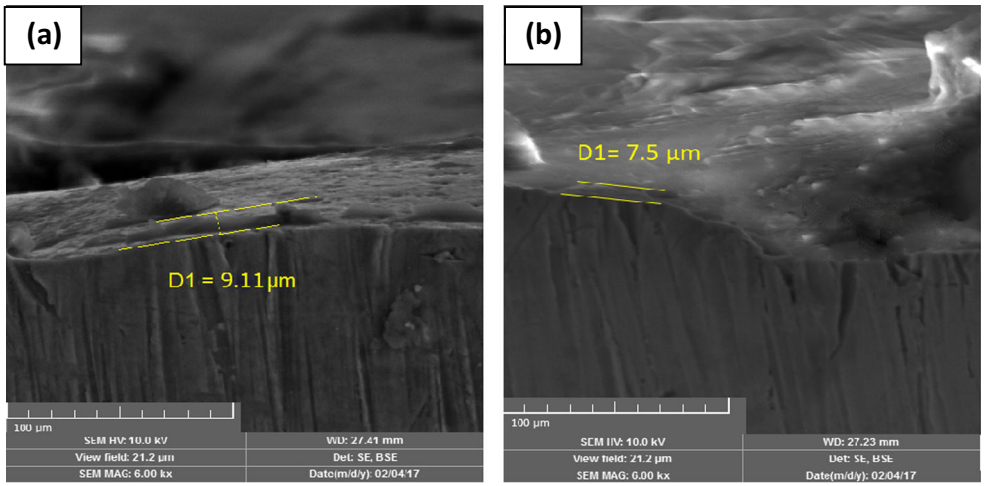

Fig. 12 Created RLT on workpiece surfaces machined by **a** EDM process and **b** MEDM process, ($I = 8$ A, $T_{on} = 12.8$ µs)

Also decreasing gap pollution by application of magnetic fields in EDM process prevents from re-solidification and re-attaching the big suspended debris in gap distance to machined surface and decreases the generated RLT.

Figure 12 shows the created RLT on machined surfaces by EDM and MEDM processes, which was obtained by experiments. The same as Fig. 11, Fig. 12 also shows that the thickness of created recast layer on machined surfaces is lower in the case of MEDM process.

4.3 Effects of application of magnetic fields in EDM process on dimensions of generated craters

Figure 13a–c, which has been obtained by numerical analysis, shows the dimensions of generated craters on machined surface induced by single discharge of EDM and MEDM at different pulse currents. According to Fig. 13, the depth and volume of craters at MEDM process is higher than EDM but radius of craters at MEDM process is smaller than EDM.

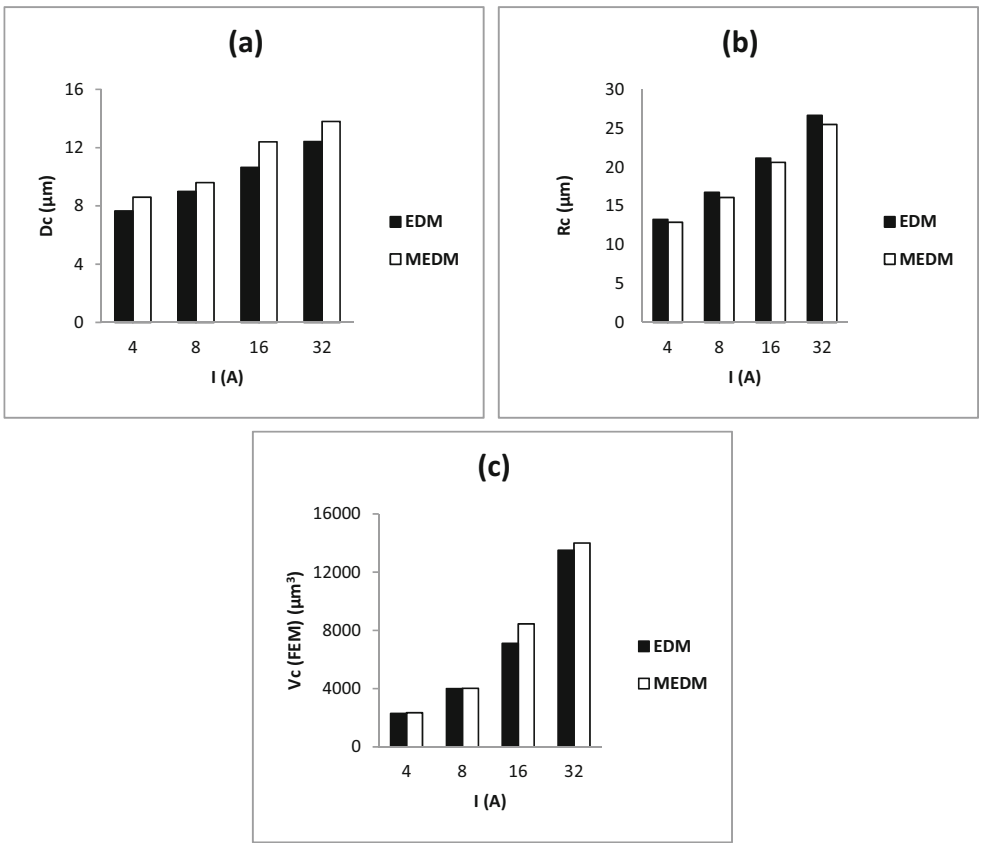

Fig. 13 **a** Depth, **b** radius, and **c** volume of generated craters, at different pulse currents ($T_{on} = 6.4$ µs) in EDM and MEDM processes

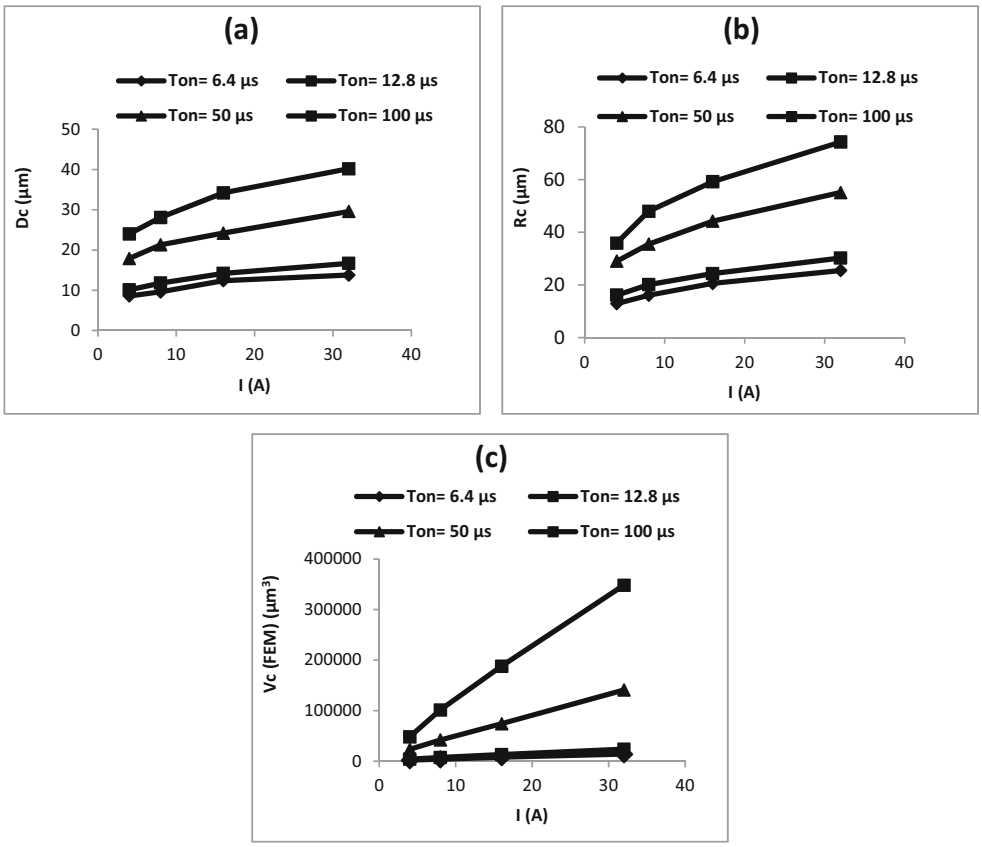

Fig. 14 Influence of pulse current and pulse on-time on **a** depth, **b** radius, and **c** volume of generated craters caused by single discharge of MEDM process

As mentioned before, plasma channel radius at MEDM process is smaller than EDM. This is because of generation of Lorentz force induced by applied magnetic field around gap distance of EDM, which confines the plasma channel radius according to Eq. 6. Also the gap pollution and so the number of arc pulses is lower in the case of MEDM process according to Fig. 10, which can also leads to lower plasma channel radius. Decreasing plasma channel radius by applying magnetic field around gap distance can lead to lower radius of generated craters. Considering these facts, it can be concluded that the current density is increased due to decrease in plasma channel radius and can lead to higher depth of generated craters.

4.4 Influence of pulse current and pulse on-time on dimensions of generated craters at MEDM process

Figure 14a–c demonstrates the dimensions of generated craters on machined surface caused by single discharge of MEDM process, which was obtained numerically. According to Fig. 14, the dimensions of generated craters on machined surface are enhanced by increasing pulse current and pulse on-times. Higher amount of heat is generated by single discharge of MEDM process in higher pulse current and on-time. So the amount of transferred heat to workpiece and consequently the amount of melted and evaporated materials (and so the depth, radius, and volume of created craters) are enhanced.

5 Conclusion

An electro-thermal model has been proposed for simulation of the MEDM process using finite element method. Mathematical modeling was also done to achieve the plasma channel radius which has been determined with empirical relations, before. Due to good agreement between numerical and empirical results of RLT with maximum error of 8.8%, the proposed finite element model was used to study the effects of application of magnetic field in EDM process on dimensions of generated craters, PFE and RLT. The main results of this investigation are as follows:

- Application of magnetic field in EDM process leads to a decrease in radius of generated craters and an increase in depth and volume of generated craters on machined surface.
- The depth, radius, and volume of generated craters caused by single discharge of MEDM process are enhanced by increasing pulse current and pulse on-time.

- Applying magnetic field around gap distance of EDM process increases PFE while decreases the amount of generated RLT in all pulse currents and pulse on-times.

References

1. Chang GW, Yan BH, Hsu RT (2002) Study on cylindrical magnetic abrasive finishing using unbonded magnetic abrasives. Int J Mach Tools Manuf 42:575–583
2. Yamaguchi H, Shinmura T (2004) Internal finishing process for alumina ceramic components by a magnetic field-assisted finishing process. Precis Eng 28:135–142
3. Kim JD (2003) Polishing of ultra-clean inner surfaces using magnetic force. Int J Adv Manuf Technol 21:91–97
4. Teimouri R, Baseri H (2012) Study of tool wear and overcut in EDM process with rotary tool and magnetic field. Advances in Tribology 2012(Article ID 895918):8
5. De Bruijn HE, Delft TH, Pekelharing AJ (1978) Effect of a magnetic field on the gap cleaning in EDM. Annals of CIRP 27:93–95
6. Teimouri R, Baseri H (2012) Effects of magnetic field and rotary tool on EDM performance. J Manuf Process 14:316–322
7. Zhao B, Xu X, Cai G, Kang R (2009) Experimental and mechanism research on EDM combined with magnetic field. Key Eng Mater 416:337–341
8. Lin YC, Lee HS (2009) Optimization of machining parameters using magnetic-force-assisted EDM based on gray relational analysis. Int J Adv Manuf Technol 42:1052–1064
9. Lin YC, Chen YF, Wang DA, Lee HS (2009) Optimization of machining parameters in magnetic force assisted EDM based on Taguchi method. J Mater Process Technol 209:3374–3383
10. Govindan P, Gupta A, Joshi SS, Malshe A, Rajurkar KP (2013) Single-spark analysis of removal phenomenon in magnetic field assisted dry EDM. J Mater Process Technol 213:1048–1058
11. Joshi S, Govindan P, Malshe A, Rajurkar K (2011) Experimental characterization of dry EDM performed in a pulsating magnetic field. CIRP annals- manufacturing. Technology 60:239–242
12. Cao MR, Geng XD (2011) Process research on high-speed small hole drilling by EDM combined with magnetic field and water dispersant. Adv Mater Res 189:269–272
13. Heinz K, Surla V, Kapoor SG, DeVor RE (2011) An investigation of magnetic-field-assisted material removal in micro EDM for non-magnetic materials. J Manuf Sci Eng 133(2):9 021002
14. Lee HT, Yur JP (2000) Characteristic analysis on EDMed surfaces using Taguchi method approach. Mater Manuf Process 15(6):781–806
15. Lee HT (1996) Influence of EDM process parameters on surface defects and roughness. Chin J Mater Sci 28(4):270–278
16. Shabgard MR, Gholipoor A, Mohammadpourfard M (2018) Numerical and experimental study of the effects of ultrasonic vibrations of tool on machining characteristics of EDM process. Int J Adv Manuf Technol 96 (5): 2657–2669
17. Van Dijck F, Dutre W (1974) Heat conduction model for the calculation of the volume of molten metal in electric discharges. J Phys D Appl Phys 7(6):899–910
18. Allen P, Chen X (2007) Process simulation of micro electro-discharge machining on molybdenum. J Mater Process Technol 186(1):346–355
19. Murali MS, Yeo SH (2005) Process simulation and residual stress estimation of micro-electro discharge machining using finite element method. Jpn J Appl Phys 44:52–54
20. Yada V, Jain VK, Dixit PM (2002) Thermal stresses due to electrical discharge machining. Int J Mach Tools Manuf 42(8):877–888
21. Rajurkar K, Pandit S (1984) Quantitative expressions for some aspects of surface integrity of electro discharge machined components. J Eng Ind (Trans. ASME) 106(2):171–177
22. Dibitonto DD (1989) Theoretical models of the electrical discharge machining process. I. A simple cathode erosion model. J Appl Phys 66(9):4095–4103
23. Yeo SH, Kurnia W, Tan PC (2007) Electro-thermal modeling of anode and cathode in micro-EDM. J Phys D Appl Phys 40:2513–2521
24. Snoeys R, Van Dijck F (1971) Investigation of electro discharge machining operations by means of thermo-mathematical model. CIRP Ann 20(1):35–37
25. Jilani TS, Pandey P (1983) An analysis of surface erosion in electrical discharge machining. Wear 84(3):275–284
26. Shabgard M, Ahmadi R, Seyedzavvar M, Bavil Oliaei SN (2013) Mathematical and numerical modeling of the effect of input-parameters on the flushing efficiency of plasma channel in EDM process. Int J Mach Tool Manu 65:79–87
27. Halliday D, Resnick R, Walker J (2013) Fundamentals of physics extended, 10th edition. John Wiley & Sons
28. Eubank PT, Patel MR, Barrufet MA, Bozkurt B (1993) Theoretical models of the electrical discharge machining process. III. The variable mass, cylindrical plasma model. J Appl Phys 73(11):7900–7909
29. Ryzko H (1965) Drift velocity of electrons and ions in dry and humid air and in water vapor. Proc Phys Soc 85(6):1283–1295
30. Descoeudres A (2006) characterization of electrical discharge machining plasmas; Ph. D Thesis; The Victoria University of Manchester
31. Francis CK, Bennett HT (1922) The surface tension of petroleum. J Indus Eng Chem 14(7):626–627
32. Wang F, Wu J, Liu Z (2006) Surface tensions of mixtures of diesel oil or gasoline and dimethoxymethane, dimethyl carbonate, or ethanol. Energy Fuel 20:2471–2474
33. Loo KH, Moss GJ, Tozer RC, Stone DA, Jinno M, Devonshire R (2004) A dynamic collisional-radiative model of a low-pressure approach to modeling fluorescent lamps for circuit simulations. IEEE Trans Power Electron 19(4):1117–1129
34. Albinskiy K, Musiol K, Miernikiewicz A, Labuz S, Malota M (1996) The temperature of a plasma used in electrical discharge machining. Plasma Sources Sci Technol 5:736–742
35. Sen SN, Das RP (1973) Effect of magnetic field on primary ionization by electron collision. Int J Electron 39(6):448–457
36. Francis F C (2016) Introduction to plasma physics and controlled fusion, 2nd Edition, Springer international publishing Switzerland
37. Salonitis K, Stournaras A, Stavropoulos P, Chryssolouris G (2009) Thermal modeling of the material removal rate and surface roughness for die-sinking EDM. Int J Adv Manuf Technol 40:316–323
38. Marafona J, Chousal JAG (2006) A finite element model of EDM based on Joule effect. Int J Mach Tool Manu 46:595–602